Characterisation of gas phase halide-acetone complexes with photoelectron spectroscopy and *ab initio* calculations

Timothy R. Corkish, Damien B. ’t Hart, Peter D. Watson, Allan J. McKinley, Duncan, A. Wild*

School of Molecular Sciences, The University of Western Australia, Crawley, Western Australia, 6009, Australia

**duncan.wild@uwa.edu.au +61 8 6488 3178*

Abstract

Anion photoelectron spectra of gas phase halide-acetone complexes ($X^{-}\cdots CH_3COCH_3$ where X=Cl, Br, I) are presented. Electron binding energies, corresponding to the electron affinities of the neutral species, are determined from experiment. Additionally, two ground state minima are predicted from MP2 calculations (with corresponding energies from CCSD(T) calculations) for each set of complexes: one C_s geometry for the anion complexes with the halide located midway between two hydrogens from each methyl group of acetone, and a C_1 neutral structure with the halogen appended to the carbonyl oxygen.

Keywords: photoelectron spectroscopy, acetone, halogen, mass spectrometry, gas phase anions

1 Graphical Abstract

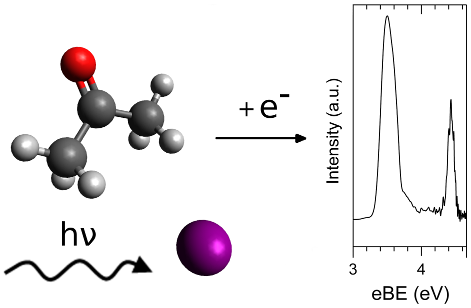

2 Introduction

The nature of intermolecular interactions between gas-phase species can be probed via spectroscopic methods, revealing insights into fundamental structures and energetics through experimental means. Anion photoelectron spectroscopy is one such technique, and can be used in tandem with mass spectrometry in order to determine the electron affinities of neutral molecules and complexes, and hence contributes to an understanding of certain intermolecular interactions. This is achieved through detaching a photoelectron from the more stable anion counterparts. In experimental conditions, the formation of gas-phase van der Waals clusters can be an important step prior to photodetachment, and so properties of ion solvation can also be investigated with this method. Provided a high enough resolution, anion photoelectron spectroscopy can derive not only electronic state information, however also vibrational information of the neutral complexes, with some recent examples of the use of this technique provided in references 1-4. The aim of the work described in the current article is to measure photoelectron spectra of halide-acetone complexes ($X^- \cdots CH_3COCH_3$ where X=Cl, Br, I) and complement the experimental results with theory, with the theoretical work extending to fluorine complexes.

The atmospheric processes involving halogens have attracted much attention due to their role in stratospheric ozone destruction.[5] Upon being produced by the photodissociation of chlorofluorocarbons (CFCs) or as a result of sea spray,[6, 7] halogen radicals catalyse this destruction, in addition to reacting with other species. Simple carbonyl molecules constitute a subset of these additional species, and understanding the nature of their specific interactions with halogen radicals can contribute to a greater understanding of fundamental atmospheric dynamics. Attention here is turned towards the specific gas-phase reactions of halogens with acetone.

Acetone has been dubbed 'the most dominant non-methane organic species' in the atmosphere and is a ubiquitous component of all its layers.[8] Sources of acetone include the oxidation of precursor hydrocarbons (such as propane), as well as direct emission from terrestrial vegetation, ocean sources, and biomass burning.[9] The photolysis of acetone is believed to be its major atmospheric sink, with estimates of 64% of degradation occurring in such a fashion.[8] Approximately 24% of this degradation is attributed to the reaction with the OH radical; the simple hydrogen abstraction resulting in products that lead to the formation of peroxyacetylnitrates, which form part of photochemical smog, as well as HO_x compounds, which are important for tropospheric ozone production.[10]

Halogens and the hydroxyl radical react very similarly with acetone; Nielsen et al. determining three pathways to be thermodynamically feasible for the case of a reaction between a Cl atom and acetone.[11]

$$\cdot \mathrm{Cl} + \mathrm{CH_3COCH_3} \longrightarrow \cdot \mathrm{CH_3COCH_2} + \mathrm{HCl} \tag{1a}$$

$$\cdot \mathrm{Cl} + \mathrm{CH_3COCH_3} \longrightarrow \mathrm{CH_3COCl} + \cdot \mathrm{CH_3} \tag{1b}$$

$$\cdot \mathrm{Cl} + \mathrm{CH_3COCH_3} \longrightarrow \cdot \mathrm{CH_3CO} + \mathrm{CH_3Cl} \tag{1c}$$

In their study, the abstraction channel of Equation 1a was found to proceed approximately 97% of the time, suggesting mechanistically that for the same reason as the acetone reaction with OH, the reaction with Cl, and by extension other halogens, is of interest. The example of Cl is of particular pertinence, especially when considering that the reaction rate between acetone and Cl is an entire order of magnitude higher than with acetone and OH ((2.2 ± 0.4) x 10^{-12} cm^3 molecule^{-1} s^{-1} compared with (2.2 ± 0.5) x 10^{-13} cm^3 molecule^{-1} s^{-1}).[12]

Computational studies have also shown the abstraction reaction to be favourable due to a small barrier height,[13] the implication being that in areas of higher Cl concentration, the 24% removal of acetone via OH is rivalled. A study by Romanias et al. suggests that the figure of tropospheric acetone removal via a reaction with Cl would approach 11%, and as such should be given more consideration with respect to atmospheric models.[14] Other halogens do not contribute to the degradation of tropospheric acetone with the same efficiency as chlorine, despite featuring the same dominant hydrogen abstraction channel, but have warranted attention in the form of computational studies of their respective reactions.[15, 16]

Anion photoelectron spectroscopy, in this work, will then provide a means of investigating the interactions between halogens and acetone and ascertain fundamental properties; most notably, electron binding energies. It is important to note here that the $I^-\cdots CH_3COCH_3$ photoelectron spectrum has been reported previously by Dessent et al. with a ${}^2P_{3/2}$ electron binding energy of approximately 3.49 eV, which corresponds to the lowest lying spin-orbit state of a perturbed bare iodine atom.[17] These previous results will be compared to our own experiments and rationalised with calculations, with Cl^-, Br^-, and I^- complexes treated both experimentally and theoretically, while F^- only computationally. A combination of time-of-flight mass spectrometry and photoelectron spectroscopy is used to characterise gas-phase clusters consisting of a halide and acetone in a 1:1 ratio to determine the electron affinities of the neutral species. Geometry optimisations, vibrational frequency analyses, and simulated electron detachment energies encompassing both anion and neutral complexes are computed using calculations at the MP2 level of theory, with additional CCSD(T) single point energies.

3 Methods

3.1 Experimental Methods

The experiments conducted in this work made use of a time of flight mass spectrometer coupled to a photoelectron spectrometer (TOF-PES), based on the design of the mass spectrometer reported by Wiley and McLaren,[18] while the magnetic bottle design of the photoelectron spectrometer was introduced by Cheshnovsky.[19] A detailed explanation of the operation of the TOF-PES can be found in other works from the Wild Group.[20]

The first step of creating gas-phase anions began by making a mixture of a halide donor species (either CCl_4, CH_2Br_2, or CH_3I), acetone, and argon together in a gas mixing chamber at a pressure of approximately 400 kPa. The liquid phase constituents, being the halide source and acetone, were introduced into the chamber via their vapour pressures. The gas mixture was pulsed into the TOF-PES by a solenoid nozzle and intersected by a beam of electrons from a rhenium filament, with anion clusters formed after a process of dissociative electron attachment.

Specific clusters or ions of interest are irradiated with a 5 ns pulse of 266 nm radiation in order to eject photoelectrons and this 4.66 eV photon is the result of the fourth harmonic of a Nd:YAG laser (Spectra Physics Quanta Ray Pro). Photoelectrons are extracted with a bottleneck-shaped magnetic field[19] and travel down a 1.8 m long flight tube, with electrons detected with a microchannel plate detector, whose front face is biased at +200 V with respect to a wire mesh screen held some 20 mm in front of the detector assembly. Photoelectron counts are measured as a function of time of flight, which upon conversion to electron kinetic energy (eKE) allows the electron binding energy (eBE) to be determined via Equation 2:

$$eBE = h\nu - eKE \tag{2}$$

where $h\nu$ is the energy of the input photon (4.66 eV). The conversion from a time-dependent intensity to one that is energy-dependent is not a straightfroward linear process, and as a result, the final intensities are multiplied by a factor of their time-of-flight (t^3). This Jacobi transform applies the necessary adjustment to move from energy bins of $\mathrm{d}t$ width to those of $\mathrm{d}E$. Prior to this, the raw spectra are recorded over 10 000 laser shots, averaged, and smoothed. Calibration spectra are also recorded of the bare halides, including residual amounts from previous experiments, in order to determine the *eBE* of unknown clusters. The $\mathrm{Cl}^-\cdots\mathrm{CH_3COCH_3}$ spectrum was calibrated using a combination of the well known electron affinities of the ${}^2P_{3/2}$ Cl state, as well as the ${}^2P_{3/2}$ and ${}^2P_{1/2}$ states of I, for example, although the appearance of the ${}^2P_{1/2}$ spin-orbit state of Cl is obscured by the limited resolution of the apparatus, given as follows:[19]

$$\mathrm{d}E_e = 4\sqrt{\frac{m_e}{m_I}E_eE_I} \tag{3}$$

where E_e and E_I are the respective kinetic energies of the detached electron and the anion, while m_e and m_I are their masses. An electron removed from a ${}^{35}\mathrm{Cl}^-$ anion (travelling in an ion beam of 1000 eV energy) would have 1.05 eV of kinetic energy after absorption of a 4.66 eV photon, resulting in a $\mathrm{d}E_e$ value of 0.51 eV. The full width half maximum of such a peak is 0.21 eV and corresponds to the resolution of the apparatus, and explains why the ${}^2P_{1/2}$ state of Cl and its related clusters is not resolved.

3.2 Computational Methods

Initial *ab initio* calculations were performed at the MP2 level of theory using Gaussian 09.[21] Dunning's augmented correlation consistent basis sets were employed; with aug-cc-pVQZ for first row atoms,[22] aug-cc-pV(Q+d)Z with additional diffuse functions for chloride,[23] and aug-cc-pVQZ PP basis sets for bromine and iodine.[24, 25] For simplicity these basis sets will be referred to henceforth as AVQZ. Following geometry optimisations and frequency analyses of anion and neutral halide-acetone complexes at MP2/AVQZ, CCSD(T) single point energy calculations were performed.

Due to the loosely bound nature of these systems, tighter convergence criteria (1×10^{-8} E_h ${a_0}^{-1}$) were used during geometry optimisations. Additionally, in order to determine the complex binding energies D_e and D_0, structures and energies of bare halide anions, halogen neutrals, and acetone were computed. Two methods of complete basis set (CBS) extrapolation were applied to the computed energies: one involving MP2 energies and the other CCSD(T). For the MP2 method, the SCF energy was extrapolated from AVQZ/AV5Z basis sets using a formula attributed to Karton and Martin,[26] shown in Equation 4. Note that L represents the cardinal number of the basis set used (i.e. 5 for AV5Z).

$$E_\infty = E_L + \frac{E_L - E_{L-1}}{\frac{L\exp(9\sqrt{L} - \sqrt{L-1})}{L+1} - 1} \tag{4}$$

Eq. (5) below, a formula used throughout various extrapolation methods, was used to extrapolate the MP2 correlation energy from AVQZ/AV5Z basis sets. A value of α=3 was chosen, as has been used in previous work.[27]

$$E_\infty = E_L + \frac{E_L - E_{L-1}}{\left(\frac{L}{L-1}\right)^\alpha - 1} \tag{5}$$

The CCSD(T) extrapolation was done in accordance with W1w protocol.[28] In short, this method involves the formula of Equation 5, extrapolating the SCF energy from AVTZ/AVQZ basis sets with α=5, CCSD contributions from AVTZ/AVQZ with α=3.22, and the (T) inclusion from AVDZ/AVTZ with α=3.22. Further details on the MP2, CCSD(T), and CBS energies included in this work can be found in the Supplementary Material.

4 Results and Discussion

4.1 Computational Results

4.1.1 Complex Geometries

Both anion and neutral halide-acetone complexes were optimised at the MP2/AVQZ level with vibrational analyses returning all real modes unless stated otherwise. It should also be noted that cartesian coordinates for each geometry featured in this work are available in the Supplementary Material attachment. All anion complexes converged to a similar stable minimum, displaying C_s symmetry with the halide equally bound to a hydrogen of each methyl group. Figure 1.a depicts this structure for the case of the $Cl^- \cdots CH_3COCH_3$ minimum, with the only difference between the halide complexes being the distance to the nearest hydrogens of CH_3COCH_3 as well as the angle made with the C=O bond. Table 1 notes the structural parameters for the anion complexes at the MP2/AVQZ level. As expected, the distance of the halide to the central C atom of acetone increases with halide size, ranging from 3.25 Å to 4.30 Å, with distances to the nearest hydrogens from 1.90 Å for the fluoride complex up to 2.87 Å for the iodide complex). There is also a slight increase in the angle made with the carbonyl bond, centred at approximately 144° for each complex. Table 1 also lists the complex dissociation energies D_e and D_0. The relatively high complex binding energies are attributed to strong ion-dipole interactions between the halide and both the carbonyl bond and nearby hydrogen atoms. This contributes to the experimental trend of large electron stabilisation energies. Increasing halide size also results in a decrease in D_e and D_0 values owing to the greater distances between the respective halide and the acetone molecule.

Both MP2 and CCSD(T) CBS dissociation energies are presented in Table 1. While there is variable agreement between the results for each halide (a difference of 0.3 kJ mol^{-1} between MP2 and CCSD(T) energies for $Cl^- \cdots CH_3COCH_3$ and up to 3.9 kJ mol^{-1} for $I^- \cdots CH_3COCH_3$), all CBS energies show the same trend with respect to halide size and proximity.

Table 1: Geometrical parameters of the C_s halide-acetone anion complexes from MP2/AVQZ calculations. The C···X distance refers to that of Figure 1.a. The two values of D_e and D_0 are those calculated from the MP2 and CCSD(T) CBS results respectively.

	$r_{C \cdots X}$ [Å]	$\angle_{O=C-X}$	D_e [kJ mol^{-1}] MP2|CCSD(T)	D_0 [kJ mol^{-1}] MP2|CCSD(T)
$F^- \cdots CH_3COCH_3$	3.252	143.2°	91.2 | 94.9	89.7 | 93.4
$Cl^- \cdots CH_3COCH_3$	3.912	144.1°	60.3 | 58.6	58.6 | 56.9
$Br^- \cdots CH_3COCH_3$	4.042	144.2°	57.3 | 57.5	55.9 | 56.2
$I^- \cdots CH_3COCH_3$	4.301	145.5°	55.4 | 51.5	54.0 | 50.2

Attempts to locate stable minima for neutral structures proved to be difficult, owing to the small interaction energies, however one minimum was found with respect to all halogen radicals complexing with an acetone molecule. An example of this structure for the $Cl \cdots CH_3COCH_3$ complex is found in Figure 1.b. The Cl radical lies slightly out of plane, and the methyl groups of acetone have undergone a slight torsion.

In reference to Figure 1.b, the dihedral angle ϕ corresponds to the $Cl-O-C_2-C_1$ plane, with the Cl atom residing at an angle of 1.2° out of plane (out of page), ψ being the dihedral angle of

$H-C_1-C_2-O$, with the methyl group rotated 12.7° into the page, and ω being the corresponding $H-C_3-C_2-O$ dihedral, this time the methyl group rotated so that the formerly planar hydrogen is placed 7.8° out of page.

The resultant C_1 structures are described by these dihedral angles, as well as distance to the carbonyl oxygen and angle made with the C=O bond in Table 2. These O···X distances again increase with halogen size, ranging from 2.35 Å to 2.78 Å, as does the angle made with the carbonyl bond, from approximately 120° to 124°.

The dihedral angles ψ, ϕ, and ω, or in other words, the extent to which the halogen resides out of plane, and subsequent torsion of each methyl group, display slightly complex trends. These angles increase in the order of F < I < Cl < Br, to the point where $F\cdots CH_3COCH_3$ is almost of C_s symmetry while one methyl group of $Br\cdots CH_3COCH_3$ is rotated up to 15.0°. It then seems appropriate to invoke a 'Goldilocks' argument with respect to halogen size, polarisability, and distance from the solvating molecule.

Table 2: Geometrical parameters of the C_1 halogen-acetone neutral complexes from MP2/AVQZ calculations. For a description of the dihedral angles ϕ, ψ, and ω see Figure 1.b. The two values of D_e and D_0 are those calculated from the MP2 and CCSD(T) CBS results respectively.

	$r_{O\cdots X}$ [Å]	$\angle_{C=O-X}$	ϕ	ψ	ω	D_e [kJ mol^{-1}] MP2|CCSD(T)	D_0 [kJ mol^{-1}] MP2|CCSD(T)
$F\cdots CH_3COCH_3$	2.354	120.4°	0.0°	-0.1°	0.1°	8.9 | 17.9	7.4 | 16.4
$Cl\cdots CH_3COCH_3$	2.480	121.4°	1.2°	-12.7°	7.8°	21.4 | 24.4	18.9 | 21.9
$Br\cdots CH_3COCH_3$	2.585	121.9°	2.6°	-15.0°	8.2°	25.2 | 29.1	22.9 | 26.9
$I\cdots CH_3COCH_3$	2.781	124.1°	1.1°	-11.1°	7.5°	30.8 | 29.5	28.9 | 27.6

That is, from fluorine to chlorine to bromine, the dihedral angles increase with increasing halogen size and polarisability, in spite of an increased distance to the acetone molecule. However, the iodine complex sees a reduction of ϕ, ψ, and ω from the bromine and chlorine complexes, despite being of a larger size and polarisability. It would then seem that the greater distance of the iodine radical results in a lowering of the methyl rotation angles. For all of the halogen complexes, it appears that bromine occupies the 'just right' position, whereby the trade-off between size, polarisability, and distance has resulted in the largest torsion angles of each of the methyl groups. A similar phenomenon has been described, albeit in relation to the dissociation energies, in order to rationalise the trends observed for neutral halogen-acetylene complexes.[29]

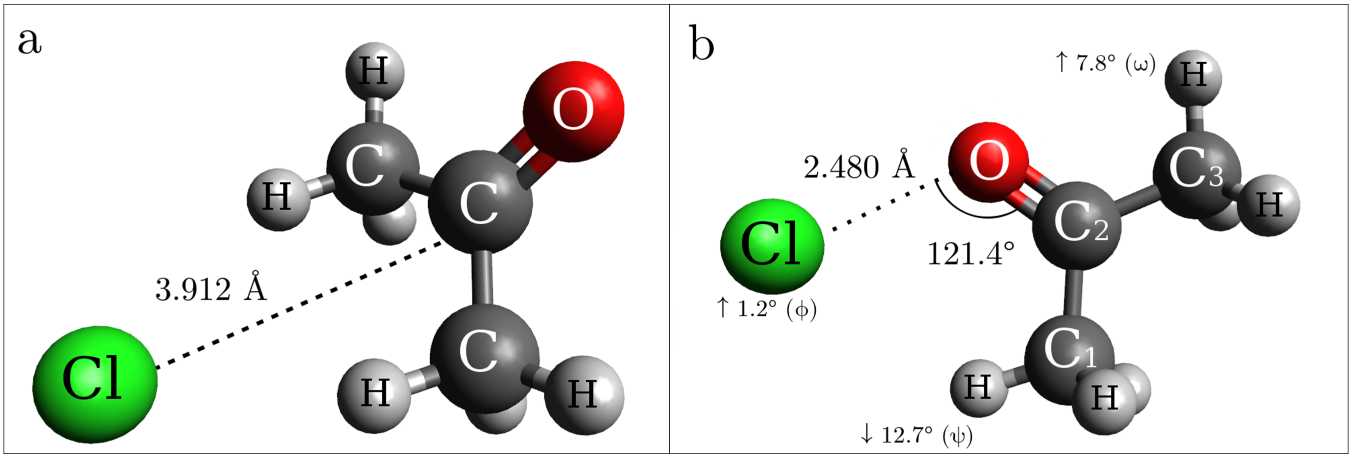

Figure 1: Geometries predicted at the MP2/AVQZ level of the (a) $Cl^{-}\cdots CH_3COCH_3$ anion complex and (b) $Cl\cdots CH_3COCH_3$ neutral complex. Structure (a) is of C_s symmetry, while structure (b) is of C_1 symmetry, with the dihedral angles ϕ, ψ, and ω referring to the $Cl-O-C_2-C_1$, $H-C_1-C_2-O$, and $H-C_3-C_2-O$ planes respectively. Up arrows refer to rotation of the bond or displacement out of page, while down arrows are into the page.

Despite the irregular trends of the dihedral angles, the dissociation energies D_e and D_0 increase with increasing halogen size for both the MP2 and CCSD(T) cases, which is opposite to the observed trend for the anions. This is to be expected as the C_1 neutral structures, depicted in Figure 1.b, are likely bound due to a large contributions from dipole induced-dipole forces, with this interaction becoming more apparent for the larger, more polarisable halogens.

The geometry of the neutral structures computed in this work could be of importance when considering the halogen-initiated hydrogen abstraction of acetone. A similar oxygen-appended geometry between halogens and formaldehyde has been previously calculated and posited to be a pre-reaction adduct involved in the related hydrogen abstraction.[30, 31] Additionally, this minimum was found to exist in the hydrogen abstraction channels of larger aldehydes as a pre-reaction adduct.[32]

In computational studies of halogen radicals abstracting a hydrogen from acetone, the oxygen-appended minima described in this work were suspected to exist as possible transition states for the reaction,[13, 16] however, at the MP2/AVQZ level, vibrational analyses showed all real frequencies for the structures in this work. These frequencies, in addition to cartesian coordinates for the neutral minima, can be found in the Supplementary Material.

As a final note on the neutral structures; one geometry with the halogen residing in a methyl pocket (i.e. making a C_2-C_1-X angle of 180.0° as per Figure 1.b) converged to a stable minimum at the MP2/aug-cc-pVDZ level, but could not be isolated at higher levels of theory.

4.1.2 Computed Detachment Energies

The predicted computational detachment energies from both MP2 and CCSD(T) CBS results are shown in Table 3. The adiabatic detachment energy (ADE) corresponds to a transition from the ground state anion to the ground state neutral minimum, while the vertical detachment energy (VDE) is a transition from the anion minimum to a neutral state of the same geometry.

The raw computational energies do not take into account spin-orbit coupling in the halogen atoms, so in order to gain an estimate for transitions to the $^2P_{3/2}$ and $^2P_{1/2}$ states, the experimental coupling constant of each halogen was added. Additionally, a shift was added based on the difference between MP2 and CCSD(T) CBS energies of the bare halide transitions to that observed by experiment. For example, using the MP2 and CCSD(T) extrapolation schemes outlined earlier, a shift of -0.150 eV was applied to the MP2 results for chloride complexes, and -0.028 eV for the same clusters at the CCSD(T) level. As can be seen from Table 3, the MP2/CBS and CCSD(T)/CBS detachment energies are in excellent agreement with one another.

Comparing the VDE and ADE values, one can see that the ADE results are consistently 2-350 meV smaller than that reported for the VDE calculations; the reason being the large difference in geometry between the ground state anion and neutral halide and halogen-acetone complexes. The Franck-Condon principle dictates that the most likely photodetachment pathway observed will be that of the VDE, and this is especially inherent in this case given the geometries of the anion and neutral complexes. As a result, it is more appropriate to compare the VDE values to the photoelectron spectra obtained via experiment.

Table 3: Summary of computational detachment energies. Both the adiabatic detachment energy (ADE) and vertical detachment energy (VDE) were calculated from MP2 and CCSD(T) calculations.

		ADE (eV)		VDE (eV)	
	CBS Energy	$^2P_{3/2}$	$^2P_{1/2}$	$^2P_{3/2}$	$^2P_{1/2}$
$F^- \cdots CH_3COCH_3$	MP2$^\alpha$	4.24	4.29	4.58	4.63
	CCSD(T)$^\beta$	4.18	4.23	4.55	4.60
$Cl^- \cdots CH_3COCH_3$	MP2	4.01	4.12	4.29	4.40
	CCSD(T)	3.96	4.07	4.29	4.40
$Br^- \cdots CH_3COCH_3$	MP2	3.69	4.15	3.92	4.38
	CCSD(T)	3.66	4.11	3.91	4.37
$I^- \cdots CH_3COCH_3$	MP2	3.31	4.25	3.55	4.49
	CCSD(T)	3.28	4.23	3.54	4.48

$^\alpha$MP2/CBS extrapolation based on AVQZ/AV5Z energies.

$^\beta$CCSD(T)/CBS extrapolation based on AVTZ/AVQZ energies. See Computational Methods for full explanation.

4.2 Experimental Results

4.2.1 Mass Spectrometry

Figure 2 depicts a mass spectrum resulting from a carbon tetrachloride, acetone, and argon gas mixture, with the largest peaks in the spectrum occurring at 35 and 37 m/z, corresponding to the isotopic masses of the bare chloride ion. Molecular species clustering to the chloride anions appear in the rest of the spectrum, resulting in a slew of peaks with a unique 3:1 splitting pattern, specifically the peaks at at 93 and 95 m/z: clusters of $Cl^{-}\cdots CH_3COCH_3$. Although not observed in the chloride spectrum, clusters involving multiple acetone solvating species (i.e. $Br^{-}\cdots(CH_3COCH_3)_2$) were observed.

Other peaks present in the mass spectrum are $Cl^{-}\cdots H_2O$ at 53 and 55 m/z, as well as $Cl^{-}\cdots N_2$ at 63 and 65 m/z. At 75 and 77 m/z are peaks attributed to $Cl^{-}\cdots Ar$ anion complexes, while small amounts of bromide and iodide are also observed. These other halides were residual amounts from previous experiments, and although only present in relatively small amounts, were able to be used to calibrate the rest of the spectrum based on their splitting patterns. The large amount of bare ^{35}Cl and ^{37}Cl suggests that cluster formation was not highly favourable in the conditions of this experiment.

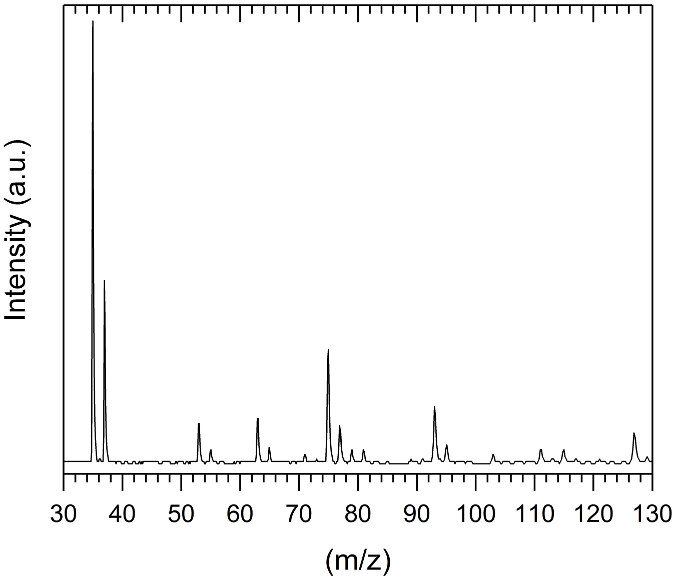

Figure 2: Mass spectrum of a gas mixture consisting of carbon tetrachloride, acetone, and argon. The main peaks to note are the isotopes of Cl^{-} at 35 and 37 m/z, as well as the $Cl^{-}\cdots CH_3COCH_3$ complex at 93 and 95 m/z.

4.2.2 Photoelectron Spectroscopy

Photoelectron spectra of the $Cl^{-}\cdots CH_3COCH_3$, $Br^{-}\cdots CH_3COCH_3$, and $I^{-}\cdots CH_3COCH_3$ complexes are presented in Figure 3, with experimentally determined electron binding energies shown in Table 4. The electron stabilisation energy, E_{stab}, refers to the difference in binding energy between the bare halide ion and the complexed species.

The bromide and iodide spectra are characterised by two major peaks, with energy distances between them consistent with the bare halide, confirming that the recorded spectra are of a halide core perturbed by a solvent molecule, rather than as a molecular entity. The larger peak of lower electron binding energy is a result of a transition to the $^2P_{3/2}$ neutral state of either Br or I, with the smaller peak of higher electron binding energy corresponding to a $^2P_{1/2}$ neutral state. The results for the $I^{-}\cdots CH_3COCH_3$ photoelectron spectrum recorded in this work are in excellent agreement with what has been previously reported.[17] Dessent et al. also reported the observation of a dipole-bound anion state occurring just prior to the photodetachment threshold, eventually dissociating into either the acetone or iodide anion via different mechanisms. This dipole-bound state was not observable in our experiment due to the input laser energy being far above the photodetachment threshold of the $I^- \cdots CH_3COCH_3$ complex. In addition, no insights can be obtained about this excited state from the calculations presented in this work.

Table 4: Experimentally determined binding energies of bare halides and halide-acetone complexes for photodetachment to the $^2P_{3/2}$ and $^2P_{1/2}$ states. Also included are the CCSD(T)/CBS vertical detachment energies to the $^2P_{3/2}$ state from Table 3 for ease of experimental comparison.

	$^2P_{3/2}$ [eV]	$^2P_{1/2}$ [eV]	E_{stab} [eV]	VDE^a [eV]
Cl^-	3.66			
$Cl^- \cdots CH_3COCH_3$	4.28		0.62	4.29
Br^-	3.36	3.81		
$Br^- \cdots CH_3COCH_3$	3.90	4.36	0.54	3.91
I^-	3.06	3.99		
$I^- \cdots CH_3COCH_3$	3.50$^\beta$	4.43	0.44	3.54
	3.49$^\gamma$		0.43	

$^\alpha$Computational values.
$^\beta$This work.
$^\gamma$Dessent et al. [17]

The two Cl spin-orbit states are not resolved in our work due to limitations in the resolution of our spectrometer and only a singular peak is observed. As a result, the E_{stab} value for $Cl^- \cdots CH_3COCH_3$ is taken from the centre of the bare chloride peak, measured at 3.66 eV in an earlier spectrum, relative to the centre of the novel chloride-acetone peak, occurring at 4.28 eV. The spectra are presented in the range of 0 to 4.66 eV on account of the input 266 nm radiation.

Also presented in Table 4 are the CCSD(T)/CBS vertical detachment energies to the $^2P_{3/2}$ state for ease of comparison (with the more detailed computational energies in Table 3). The theoretical VDEs are in very close agreement with the experimental electron binding energies, although are slightly higher than determined by experiment for the chloride and iodide systems. The MP2/CBS results shown in Table 3 are also in good agreement, and both the MP2 and CCSD(T) computational results are consistent with the experimental data. Although no experimental spectra were recorded for $F^- \cdots CH_3COCH_3$, given that the computational results consistently agree with those from experiment, the predicted detachment energies from Table 3 are likley to provide a suitable estimate for photoelectron experiments on this system.

The large electron stabilisation energies are due to the solvation of the bare halide by an acetone molecule, or in other words, clustering with acetone serves to stabilise the charge on the anion. An alternative way of rationalising the large E_{stab} values is to then compare the D_0 energies of the anion and neutral complexes. Looking to Tables 1 and 2, it can be seen that the anion species have relatively large D_0 values, especially when compared to the neutral clusters. Therefore it would be expected that a halide complexing with an acetone molecule would result in a large shift in electron binding energy. Additionally, the trend of the D_0 energies for the anions is $I^- < Br^- < Cl^- < F^-$, while the opposite is true for the neutral D_0 energies. Thus the decreasing E_{stab} values with larger halide size, as shown in Table 4, can be rationalised by the anion complex becoming less stable as halide size increases, with the neutral species becoming more so.

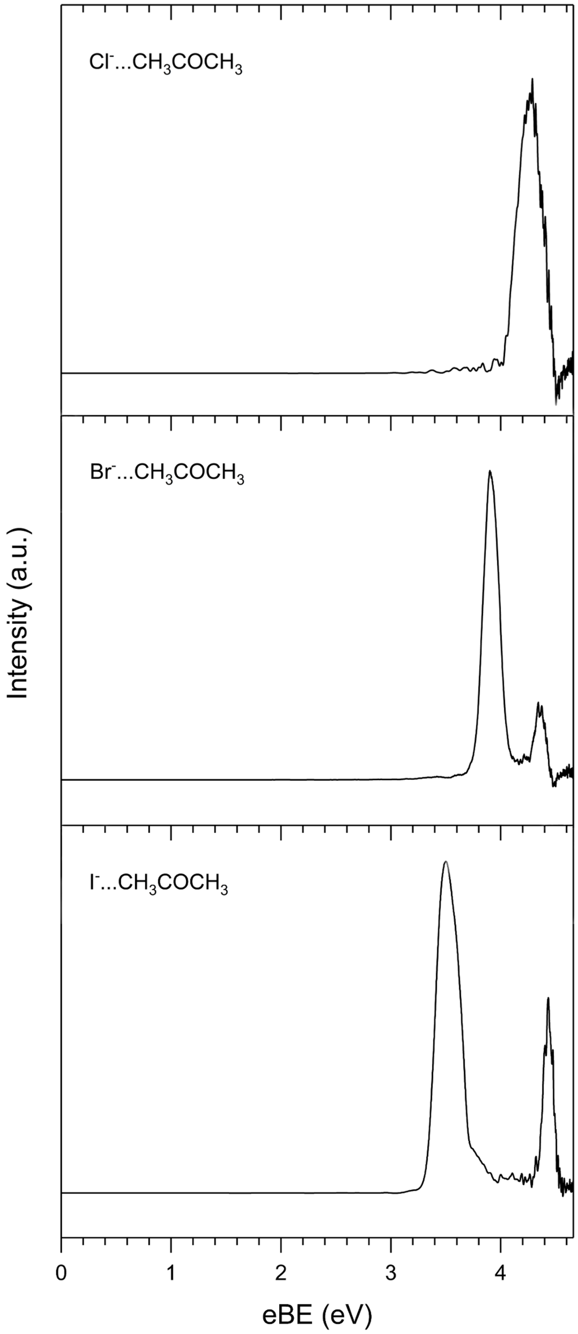

Figure 3: Anion photoelectron spectra of the chloride, bromide, and iodide-acetone gas phase complexes recorded with a photon energy of 4.66 eV.

5 Summary

Photoelectron spectra have been presented for halide-acetone clusters including $Cl^{-}\cdots CH_3COCH_3$, $Br^{-}\cdots CH_3COCH_3$, and $I^{-}\cdots CH_3COCH_3$. Electron binding energies for these clusters, which are equivalent to the electron affinities of the neutral species, have been reported. The spectra are characterised by large electron stabilisation energies on the order of 0.62 eV, 0.54 eV, and 0.44 eV for the chloride, bromide, and iodide complexes respectively.

Additionally, geometries were optimised for both the anion and neutral species at the MP2/AVQZ level (including F^{-} complexes). One stable anion minimum was found for each halide, corresponding to a C_s structure with the halide located midway between two hydrogens from each methyl group of acetone. A similar C_1 neutral structure was found for each halogen-acetone complex, consisting of the halogen appended to the carbonyl oxygen and resultant methyl rotations. These neutral structures could be important in consideration of the hydrogen abstraction of acetone via a halogen radical; however, they were not accessed via an experimental photodetachment pathway, owing to the large geometry change between the ground state anion and neutral species. Instead, the computational VDEs provide the more appropriate and direct comparison to the experimental results. Dissociation energies are also presented for each complex. Energies calculated at both MP2 and CCSD(T) were extrapolated to the CBS limit, with resulting detachment energies providing excellent experimental agreement.

6 Acknowledgements

This research was undertaken with the assistance of computational resources from the Pople high-performance computing cluster of the Faculty of Science at the University of Western Australia. The School of Molecular Sciences and the Faculty of Science are thanked for financial support, and the Australian Research Council is acknowledged for funding the laser installation under the LIEF scheme (LE110100093). T.R.C. acknowledges an Australian Government Research Training Program (RTP) scholarship, and P.D.W. thanks the support of the Center for Materials Crystallography at Aarhus University in Denmark, funded by the Danish National Research Foundation (DNRF93).

7 Supplementary Material

- In depth structures and energetics of halide-acetone and halogen-acetone complexes, as well as vibrational modes and Cartesian coordinates

8 References

[1] Kunin, A.; Li, W-L.; Neumark, D. M. Time resolved photoelectron imaging of iodide-nitromethane ($I^{-}\,.\,CH_3NO_2$) photodissociation dynamics. *Phys. Chem. Chem. Phys.* **2016**, *48*, 33226-33232. DOI: 10.1039/c6cp06646a

[2] DeVine, J. A.; Weichman, M. L.; Lyle, S. J.; Neumark, D. M. High resolution photoelectron imaging of cryogenically cooled α- and β-furanyl anions. *J. Mol. Spec.* **2017**, *332*, 16-21. DOI: 10.1016/j.jms.2016.09.002

[3] Lehman, J. H.; Lineberger, W. C. Photoelectron spectroscopy of the thiazate (NSO^-) and thionitrite (SNO^-) isomer anions. *J. Chem. Phys.* **2017**, *147*, 013943. DOI: 10.1063/1.4984129

[4] Oliveira, A. M.; Lehman, J. H.; McCoy, A. B.; Lineberger, W. C. Photoelectron spectroscopy of *cis*-nitrous acid anion (*cis*-$HONO^-$). *J. Phys. Chem. A* **2016**, *120*, 1652-1660. DOI: 10.1021/acs.jpca.5b11797

[5] Solomon, S. Progress towards a quantitative understanding of Antarctic ozone depletion. *Nature.* **1990**, *347*, 347-353. DOI: 10.1038/347347a0

[6] Molina, M.J.; Rowland, F.S. Stratospheric sink for chlorofluoromethanes: chlorine atom-catalysed destruction of ozone. *Nature.* **1974**, *249*, 810-812. DOI: 10.1038/249810a0

[7] Kritz, M. A.; Rancher, J. Circulation of Na, Cl, and Br in the tropical marine atmosphere. *J. Geophys. Res. Oceans*, **1980**, *85*, 1633-1639. DOI: 10.1029/JC085iC03p01633

[8] Singh, H. B.; O'Hara, D.; Herlth, D.; Sachse, W.; Blake, D. R.; Bradshaw, J. D.; Kanakidou, M.; Crutzen, P. J. Acetone in the atmosphere: distribution, sources, and sinks. *J. Geophys. Res.* **1994**, *99*, 1805-1819. DOI: 10.1029/93JD00764

[9] Jacob, D. J.; Field, B. D.; Jin, E. M.; Bey, I.; Li, Q.; Logan, J. A.; Yantosca, R. M.; Singh, H. B. Atmospheric budget of acetone. *J. Geophys. Res.* **2002**, *107*, ACH 5-1ACH 5-17. DOI: 10.1029/2001JD000694

[10] Jaelge, L.; Jacob, D. J.; Brune, W. H.; Wennberg, P. O. Chemistry of HO_x radicals in the upper troposphere. *Atmos. Environ.*, **2001**, *35*, 469-489. DOI: 10.1016/S1352-2310(00)00376-9

[11] Nielsen, O. J.; Johnson, M. S.; Wallington, T. J.; Christensen, L. K.; Platz, J. UV absorption spectra of HO_2, CH_3O_2, $C_2H_5O_2$, and $CH_3C(O)CH_2O_2$ radicals and mechanism of the reactions of F and Cl atoms with $CH_3C(O)CH_3$. *Int. J. Chem. Kinet.* **2002**, *34*, 283-291. DOI: 10.1002/kin.10037

[12] Carr, S.; Shallcross, D. E.; Canosa-Mas, C. E.; Wenger, J. C.; Sidebottom, H. W.; Treacy, J. J.; Wayne, R. P. A kinetic and mechanistic study of the gas-phase reactions of OH radicals and Cl atoms with some halogenated acetones and their atmospheric implications. *Phys. Chem. Chem. Phys.* **2003**, *5*, 3874- 3883. DOI: 10.1039/b304298g

[13] Tiu, G. C.; Tao, F. Theoretical mechanisms and kinetics of the hydrogen abstraction reaction of acetone by chlorine radical. *Chem. Phys. Lett.* **2006**, *428*, 42-48. DOI: 10.1016/j.cplett.2006.07.007

[14] Romanias, M. N.; Stefanopoulos, V. G.; Papanastasiou, D. K.; Papadimitriou, V. C.; Papagiannakopolous. Temperature-dependent rate coefficients and mechanism for the gas-phase reaction of chlorine atoms with acetone. *J. Chem. Kinet.* **2010**, *42*, 724-734. DOI: 10.1002/kin.20517

[15] Zhang, H.; Zhang, G.; Liu, J.; Sun, M.; Liu, B.; Li, Z. Theoretical studies and rate constants calculation for the reactions of acetone with fluorine and bromine atoms. *Theor. Chem. Acc.* **2011**, *128*, 317-325. DOI: 0.1007/s00214-010-0848-x

[16] Li, Y.; Li, H.; Hou, H.; Wang, B. Computational study of the reaction of fluorine atom with acetone. *J. Phys. Chem. A.* **2005**, *109*, 3166-3173. DOI: 10.1021/jp044086k

[17] Dessent, C. E. H.; Bailey, C. G.; Johnson, M. A. Observation of the dipole-bound excited state of the $I^- \cdot$acetone ion-molecule complex. *J. Chem. Phys.* **1995**, *102*, 6335-6338. DOI: 10.1063/1.469079

[18] Wiley, W. C.; McLaren, I. H. Time-of-flight mass spectrometer with improved Resolution. *Rev. Sci. Instrum.* **1955**, *26*, 1150-1157. DOI:10.1063/1.1715212.

[19] Cheshnovsky, O. H.; Yang, S. H.; Pettiette, C. L.; Craycraft, M. J.; Smalley, R. E. Magnetic time-of-flight photoelectron spectrometer for mass-selected negative cluster ions. *Rev. Sci. Instrum.* **1987**, *58*, 2131-2137. DOI:10.1063/1.1139475.

[20] Lapere, K. M.; LaMacchia, R. L.; Quak, L. H.; McKinley, A. J.; Wild, D. A. Anion photoelectron spectroscopy and *ab initio* calculations of the gas phase chloride-carbon monoxide complex: $Cl^- \cdots CO$. *Che. Phys. Lett.* **2011**, *504*, 13-19. DOI: 10.1016/j.cplett.2011.01.034

[21] Frisch, M. J.; Trucks, G. W.; Schlegel, H. B.; Scuseria, G. E.; Robb, M. A.; Cheeseman, J. R.; Scalmani, G.; Barone, V.; Mennucci, B.; Petersson, G. A.; Nakatsuji, H.; Caricato, M.; Li, X.; Hratchian, H. P.; Izmaylov, A. F.; Bloino, J.; Zheng, G.; Sonnenberg, J. L.; Hada, M.; Ehara, M.; Toyota, K.; Fukuda, R.; Hasegawa, J.; Ishida, M.; Nakajima, T.; Honda, Y.; Kitao, O.; Nakai, H.; Vreven, T.; Montgomery Jr., J. A.; Peralta, J. E.; Ogliaro, F.; Bearpark, M.; Heyd, J. J.; Brothers, E.; Kudin, K. N.; Staroverov, V. N.; Kobayashi, R.; Normand, J.; Raghavachari, K.; Rendell, A.; Burant, J. C.; Iyengar, S. S.; Tomasi, J.; Cossi, M.; Rega, N.; Millam, J. M.; Klene, M.; Knox, J. E.; Cross, J. B.; Bakken, V.; Adamo, C.; Jaramillo, J.; Gomperts, R.; Stratmann, R. E.; Yazyev, O.; Austin, A. J.; Cammi, R.; Pomelli, C.; Ochterski, J. W.; Martin, R. L.; Morokuma, K.; Zakrzewski, V. G.; Voth, G. A.; Salvador, P.; Dannenberg, J. J.; Dapprich, S.; Daniels, A. D.; Farkas, Ö.; Foresman, J. B.; Ortiz, J. V.; Cioslowski, J.; Fox, D. J. Gaussian 09 Revision D.01, Gaussian Inc., Wallingford CT, 2013.

[22] Kendall, R. A.; Dunning, Jr., T. H.; Harrison, R. J. Electron affinities of the first-row atoms revisited. Systematic basis sets and wave functions. *J. Chem. Phys.* **1992**, *96*, 6796-6806. DOI: 10.1063/1.462569

[23] Dunning, Jr., T. H.; Peterson, K. A.; Wilson, A. K. Gaussian basis sets for use in correlated molecular calculations. X. The atoms aluminum through argon revisited *J. Chem. Phys.* **2001**, *114*, 9244-9253. DOI: 10.1063/1.1367373

[24] Peterson, K. A.; Figgen, D.; Goll, E.; Stoll, H.; Dolg, M. Systematically convergent basis sets with relativistic pseudopotentials. II. Small-core pseudopotentials and correlation consistent basis sets for the post-d group 16-18 elements. *J. Chem. Phys.* **2003**, *119*, 11113. DOI: 10.1063/1.1622924

[25] Peterson, K. A.; Shepler, B. C.; Figgen, D.; Stoll, H. On the spectroscopic and thermochemical properties of ClO, BrO, IO, and their anions. *J. Phys. Chem. A* **2006**, *110*, 13877. DOI: 10.1021/jp065887l

[26] Karton, A.; Martin, J. M. L. Comment on: Estimating the Hartree-Fock limit from finite basis set calculations [Jensen F (2005) Theor Chem Acc 113:267]. *Theor. Chem. Acc.* **2006**, *115*, 330-333. DOI: 10.1007/s00214-005-0028-6

[27] Helgaker, T.; Klopper, W.; Koch, H.; Noga, J. Basis-set convergence of correlated calculations on water. *J. Chem. Phys.* **1997**, *106*, 9639-9646. DOI: 10.1063/1.473863

[28] Boese, A. D.; Oren, M.; Atasoylu, O.; Martin, J. M. L.; Kállay, M.; Gauss, J. W3 theory: Robust computational thermochemistry in the kJ/mol accuracy range. *J. Chem. Phys.* **2004**, *120*, 4129-4141. DOI: 10.1063/1.1638736

[29] Beckham, D. A. R.; Conran, S.; Lapere, K. M.; Kettner, M.; McKinley, A. J.; Wild D. A. Anion photoelectron spectroscopy and high level ab initio calculations of the halide-acetylene dimer complexes. *Chem. Phys. Lett.* **2015**, *619*, 241-246. DOI: 10.1016/j.cplett.2014.11.058

[30] Beukes, J. A.; D'anna, B.; Bakken, V.; Nielsen C. J. Experimental and theoretical study of the F, Cl and Br reactions with formaldehyde and acetaldehyde. *Phys. Chem. Chem. Phys.* **2000**, *2*, 4049-4060. DOI: 10.1039/b004546m

[31] Gruber-Stadler, M.; Mühläuser, M.; Sellevåg, S. R.; Nielsen, C. J. A quantum chemistry study of the Cl atom reaction with formaldehyde. *J. Phys. Chem. A* **2008**, *112*, 9-22. DOI: 10.1021/jp0753833

[32] Srinivasulu, G.; Rajakumar, B. Rate coefficients for hydrogen abstraction reection of pinonaldehyde ($C_{10}H_{16}O_2$) with Cl atoms between 200 and 400 K: a DFT study. *J. Chem. Sci.*, **2016**, *128*, 977-989. DOI: 10.1007/s12039-016-1075-3

SUPPLEMENTARY MATERIAL

The supporting information presented here comprises results of *ab initio* calculations performed on halide and halogen-acetone gas phase complexes. Included are structures, energies, vibrational data, and cartesian coordinates predicted at the MP2 and CCSD(T) levels of theory, with aug-cc-pVDZ, TZ, QZ, and 5Z basis sets. The aug-cc-pV(X+d)Z basis set was employed for chlorine, while the aug-cc-pVXZ PP basis sets were used for bromine and iodine. Collectively, these basis sets will be referred to as AVXZ.

1 Structures and Energetics

Table S1: Energies of the bare acetone molecule, halide anions, and halogen radicals determined from MP2 calculations.

		$E_{(MP2)}$ [E_h]	zpe [kJ mol^{-1}]	VDE [eV]	Experimental SO* [eV]	Split [eV]	Literature $^2P_{3/2}$ VDE † [eV]	Shift ‡ [eV]
Acetone	AVTZ	-192.7901137	221.3					
	AVQZ	-192.8453177						
	AV5Z	-192.8648886						
	CBS	-192.8829849						
F$^-$ | F	AVTZ	-99.7458784 | -99.6121061		3.640		3.623 | 3.673		-0.222
	AVQZ	-99.7744066 | -99.6379766		3.713		3.696 | 3.746		-0.295
	AV5Z	-99.7855563 | -99.6480512		3.742		3.725 | 3.775		-0.324
	CBS	-99.7956685 | -99.6568560		3.777	-0.017 | +0.033	3.760 | 3.810	3.401	-0.359
Cl$^-$ | Cl	AVTZ	-459.7815402 | -459.6479840		3.634		3.598 | 3.707		+0.015
	AVQZ	-459.8030837 | -459.6662773		3.723		3.687 | 3.796		-0.074
	AV5Z	-459.8115678 | -459.6734347		3.756		3.720 | 3.829		-0.107
	CBS	-459.8200810 | -459.6804894		3.799	-0.036 | +0.073	3.763 | 3.872	3.613	-0.150
Br$^-$ | Br	AVTZ	-415.8182646 | -415.6917550		3.443		3.291 | 3.748		+0.073
	AVQZ	-415.8967867 | -415.7667885		3.576		3.424 | 3.881		-0.060
	AV5Z	-415.9841344 | -415.8526228		3.579		3.427 | 3.884		-0.063
	CBS	-416.0757135 | -415.9425462		3.624	-0.152 | +0.305	3.472 | 3.929	3.364	-0.108
I$^-$ | I	AVTZ	-294.9658305 | -294.8458971		3.264		2.950 | 3.892		+0.109
	AVQZ	-295.0462741 | -294.9223505		3.372		3.058 | 4.000		+0.001
	AV5Z	-295.1063149 | -294.9806913		3.418		3.104 | 4.046		-0.045
	CBS	-295.1692875 | -295.0417877		3.470	-0.314 | +0.628	3.156 | 4.098	3.059	-0.097

* Values from http://www.nist.gov/pml/data/handbook/index.cfm

† Values from http://webbook.nist.gov

‡ Shift refers to the difference between the predicted and literature Electron Detachment Energy

Table S2: Energies of the bare acetone molecule, halide anions, and halogen radicals determined from CCSD(T) calculations

		$E_{\text{(CCSD(T))}}$ [E_h]	zpe [kJ mol^{-1}]	VDE [eV]	Experimental SO* [eV]	Split [eV]	Literature $^2P_{3/2}$ VDE † [eV]	Shift ‡ [eV]
Acetone	AVDZ	-192.6770068	221.3					
	AVTZ	-192.8517061						
	AVQZ	-192.9009261						
	CBS	-192.9289978						
F$^-$ | F	AVDZ	-99.6686338 | -99.5500694		3.226		3.209 | 3.259		+0.192
	AVTZ	-99.7495375 | -99.6278270		3.312		3.295 | 3.345		+0.106
	AVQZ	-99.7770729 | -99.6529080		3.379		3.362 | 3.412		+0.039
	CBS	-99.7927456 | -99.6667190		3.429	-0.017 | +0.033	3.412 | 3.462	3.401	-0.011
Cl$^-$ | Cl	AVDZ	-459.7437995 | -459.6180747		3.421		3.385 | 3.494		+0.228
	AVTZ	-459.8066265 | -459.6778578		3.504		3.468 | 3.577		+0.145
	AVQZ	-459.8283951 | -459.6958913		3.606		3.570 | 3.679		+0.043
	CBS	-459.8414270 | -459.7062785		3.678	-0.036 | +0.073	3.642 | 3.751	3.613	-0.029
Br$^-$ | Br	AVDZ	-415.7264356 | -415.6061898		3.272		3.120 | 3.577		+0.244
	AVTZ	-415.8364248 | -415.7132790		3.351		3.199 | 3.656		+0.165
	AVQZ	-415.9123554 | -415.7853270		3.457		3.305 | 3.762		+0.059
	CBS	-415.9599324 | -415.8302299		3.529	-0.152 | +0.305	3.377 | 3.834	3.364	-0.013
I$^-$ | I	AVDZ	-294.8832577 | -294.7690618		3.107		2.793 | 3.735		+0.266
	AVTZ	-294.9822875 | -294.8654128		3.180		2.866 | 3.808		+0.193
	AVQZ	-295.0612422 | -294.9399753		3.300		2.986 | 3.928		+0.073
	CBS	-295.1101156 | -294.9859544		3.379	-0.314 | +0.628	3.065 | 4.007	3.059	-0.006

* Values from `http://www.nist.gov/pml/data/handbook/index.cfm`

† Values from `http://webbook.nist.gov`

‡ Shift refers to the difference between the predicted and literature Electron Detachment Energy

Table S3: Structural parameters of the C_s halide-acetone gas phase anion complexes predicted from MP2 calculations.

		$r_{\mathrm{C\cdots X}}$* [Å]	$\angle_{\mathrm{O=C-X}}$ [°]	E$_{\mathrm{(MP2)}}$ [E_h]	zpe [kJ mol^{-1}]	D$_e$ [kJ mol^{-1}]	D$_0$† [kJ mol^{-1}]	VDE† [eV]	ADE† [eV]
$F^- \cdots CH_3COCH_3$	AVTZ			-292.5713742					
	AVQZ	3.252	143.2	-292.6549686	222.7				
	AV5Z			-292.6854109					
	CBS			-292.7133758		91.2	89.7	4.58 | 4.63	4.24 | 4.29
$Cl^- \cdots CH_3COCH_3$	AVTZ			-652.5951479					
	AVQZ	3.912	144.1	-652.6715355	223.0				
	AV5Z			-652.6995045					
	CBS			-652.7260369		60.3	58.6	4.29 | 4.40	4.01 | 4.12
$Br^- \cdots CH_3COCH_3$	AVTZ			-608.6318232					
	AVQZ	4.042	144.2	-608.7653089	222.6				
	AV5Z			-608.8715428					
	CBS			-608.9805099		57.3	55.9	3.92 | 4.38	3.69 | 4.15
$I^- \cdots CH_3COCH_3$	AVTZ			-487.7769384					
	AVQZ	4.301	145.5	-487.9127125	222.6				
	AV5Z			-487.9923014					
	CBS			-488.0733556		55.4	54.0	3.55 | 4.49	3.31 | 4.25

* In this table C refers to the carbonyl C atom of acetone

† Determined using MP2/CBS energies and MP2/AVQZ zpe

Table S4: Structural parameters of the C_s halide-acetone gas phase anion complexes predicted from CCSD(T) calculations.

		$E_{(\mathrm{CCSD(T)})}$ $[E_h]$	D_e [kJ mol^{-1}]	D_0* [kJ mol^{-1}]	VDE* [eV]	ADE* [eV]
$F^{-}\cdots CH_3COCH_3$	AVDZ	-292.3819187				
	AVTZ	-292.6377544				
	AVQZ	-292.7141925				
	CBS	-292.7578797	94.9	93.4	4.55 | 4.60	4.18 | 4.23
$Cl^{-}\cdots CH_3COCH_3$	AVDZ	-652.4439354				
	AVTZ	-652.6814632				
	AVQZ	-652.7519155				
	CBS	-652.7927444	58.6	56.9	4.29 | 4.40	3.96 | 4.07
$Br^{-}\cdots CH_3COCH_3$	AVDZ	-608.4254620				
	AVTZ	-608.7109094				
	AVQZ	-608.8354855				
	CBS	-608.9108294	57.5	56.2	3.91 | 4.37	3.66 | 4.11
$I^{-}\cdots CH_3COCH_3$	AVDZ	-487.5799454				
	AVTZ	-487.8542672				
	AVQZ	-487.9820376				
	CBS	-488.0587390	51.5	50.2	3.54 | 4.48	3.28 | 4.23

* Determined using CCSD(T)/CBS energies and MP2/AVQZ zpe

Table S5: Structural parameters of the C_1 halogen-acetone gas phase neutral complexes predicted from MP2 calculations.

		$r_{\mathrm{O}\cdots\mathrm{X}}$ [Å]	$\angle_{\mathrm{C=O-X}}$* [°]	$\mathrm{E}_{(\mathrm{MP2})}$ [E_h]	zpe* [kJ mol^{-1}]	D$_e$ [kJ mol^{-1}]	D$_0$† [kJ mol^{-1}]
F···CH_3COCH_3	AVTZ			-292.4059530			
	AVQZ	2.354	120.4	-292.4869618	222.7		
	AV5Z			-292.5164237			
	CBS			-292.5432244		8.9	7.4
Cl···CH_3COCH_3	AVTZ			-652.4458240			
	AVQZ	2.480	121.4	-652.5195166	223.7		
	AV5Z			-652.5463397			
	CBS			-652.5716108		21.4	18.9
Br···CH_3COCH_3	AVTZ			-608.4917711			
	AVQZ	2.585	121.9	-608.6225851	223.5		
	AV5Z			-608.7275488			
	CBS			-608.8351115		25.2	22.9
I···CH_3COCH_3	AVTZ			-487.6462753			
	AVQZ	2.781	124.1	-487.7789501	223.1		
	AV5Z			-487.8570815			
	CBS			-487.9365047		30.8	28.9

* In this table C refers to the carbonyl C atom of acetone

† Determined using MP2/CBS energies and MP2/AVQZ zpe

Table S6: Structural parameters of the C_1 halogen-acetone gas phase neutral complexes predicted from CCSD(T) calculations.

		$E_{(CCSD(T))}$ $[E_h]$	D_e [kJ mol^{-1}]	D_0* [kJ mol^{-1}]
F···CH_3COCH_3	AVDZ	-292.2344608		
	AVTZ	-292.4865163		
	AVQZ	-292.7141925		
	CBS	-292.6025172	94.9	93.4
Cl···CH_3COCH_3	AVDZ	-652.3043883		
	AVTZ	-652.5384196		
	AVQZ	-652.6059855		
	CBS	-652.6445756	58.6	56.9
Br···CH_3COCH_3	AVDZ	-608.2932297		
	AVTZ	-608.5752531		
	AVQZ	-608.6970519		
	CBS	-608.7703268	57.5	56.2
I···CH_3COCH_3	AVDZ	-487.4558239		
	AVTZ	-487.7270951		
	AVQZ	-487.8516749		
	CBS	-487.9261796	51.5	50.2

* Determined using CCSD(T)/CBS energies and MP2/AVQZ zpe

2 Vibrational Data

Table S7: Vibrational frequencies for the C_s fluoride and chloride-acetone anion complexes from MP2/AVQZ calculations. Frequencies in cm^{-1}, zero point energies (zpe) in kJ mol^{-1}.

	Symmetry	$F^-\cdots CH_3COCH_3$	Symmetry	$Cl^-\cdots CH_3COCH_3$
ω_1	a'	3170	a'	3183
ω_2	a''	3168	a''	3181
ω_3	a'	3095	a'	3116
ω_4	a''	3088	a''	3110
ω_5	a'	2886	a'	3009
ω_6	a''	2848	a''	3001
ω_7	a'	1727	a'	1735
ω_8	a'	1506	a'	1499
ω_9	a''	1489	a'	1482
ω_{10}	a'	1486	a''	1477
ω_{11}	a''	1450	a''	1464
ω_{12}	a''	1409	a''	1410
ω_{13}	a'	1402	a'	1397
ω_{14}	a''	1247	a''	1259
ω_{15}	a'	1125	a'	1122
ω_{16}	a'	1107	a'	1099
ω_{17}	a''	933	a''	923
ω_{18}	a''	894	a''	891
ω_{19}	a'	824	a'	820
ω_{20}	a''	527	a''	531
ω_{21}	a'	515	a'	500
ω_{22}	a'	411	a'	392
ω_{23}	a'	288	a'	221
ω_{24}	a''	236	a''	163
ω_{25}	a'	211	a'	128
ω_{26}	a''	118	a''	112
ω_{27}	a'	78	a'	56
zpe		222.7		223.0

Table S8: Vibrational frequencies for the C_s bromide and iodide-acetone anion complexes from MP2/AVQZ calculations. Frequencies in cm^{-1}, zero point energies (zpe) in kJ mol^{-1}.

	Symmetry	$Br^-\cdots CH_3COCH_3$	Symmetry	$I^-\cdots CH_3COCH_3$
ω_1	a'	3184	a'	3187
ω_2	a''	3182	a''	3186
ω_3	a'	3117	a'	3122
ω_4	a''	3111	a''	3117
ω_5	a'	3011	a'	3025
ω_6	a''	3005	a''	3022
ω_7	a'	1736	a'	1738
ω_8	a'	1497	a'	1497
ω_9	a'	1480	a'	1478
ω_{10}	a''	1475	a''	1473
ω_{11}	a''	1464	a''	1466
ω_{12}	a''	1409	a''	1408
ω_{13}	a'	1396	a'	1394
ω_{14}	a''	1259	a''	1260
ω_{15}	a'	1122	a'	1121
ω_{16}	a'	1098	a'	1097
ω_{17}	a''	921	a''	918
ω_{18}	a''	890	a''	890
ω_{19}	a'	819	a'	818
ω_{20}	a''	531	a''	532
ω_{21}	a'	498	a'	496
ω_{22}	a'	390	a'	387
ω_{23}	a'	213	a'	204
ω_{24}	a''	148	a''	143
ω_{25}	a'	103	a''	101
ω_{26}	a''	102	a'	90
ω_{27}	a'	50	a'	45
zpe		222.6		222.6

Table S9: Vibrational frequencies for the C_1 halogen-acetone neutral complexes from MP2/AVQZ calculations. Frequencies in cm^{-1}, zero point energies (zpe) in kJ mol^{-1}. All mode symmetries are a.

	F$\cdots$CH$_3$COCH$_3$	Cl$\cdots$CH$_3$COCH$_3$	Br$\cdots$CH$_3$COCH$_3$	I$\cdots$CH$_3$COCH$_3$
ω_1	3215	3216	3211	3210
ω_2	3208	3211	3210	3204
ω_3	3162	3163	3163	3162
ω_4	3156	3158	3158	3157
ω_5	3080	3079	3078	3077
ω_6	3075	3075	3074	3072
ω_7	1761	1761	1757	1751
ω_8	1506	1503	1502	1502
ω_9	1483	1483	1482	1482
ω_{10}	1481	1476	1474	1475
ω_{11}	1474	1472	1473	1472
ω_{12}	1400	1400	1400	1401
ω_{13}	1390	1390	1389	1390
ω_{14}	1259	1262	1263	1263
ω_{15}	1121	1119	1118	1119
ω_{16}	1089	1089	1087	1089
ω_{17}	903	917	920	915
ω_{18}	890	897	896	896
ω_{19}	811	814	813	814
ω_{20}	541	551	548	545
ω_{21}	485	486	485	486
ω_{22}	382	386	386	385
ω_{23}	139	149	138	133
ω_{24}	110	132	128	118
ω_{25}	77	108	108	92
ω_{26}	29	76	75	69
ω_{27}	12	34	30	21
zpe	222.7	223.7	223.5	223.1

3 Cartesian Coordinates

Table S10: Cartesian coordinates of the geometries of fluoride and chloride-acetone complexes optimised at MP2/AVQZ, in Å.

		$F^{-}\cdots CH_3COCH_3$			$Cl^{-}\cdots CH_3COCH_3$		
		x	y	z	x	y	z
C_s Anion	C	0.225201	0.816788	0.000000	0.272183	-1.434251	0.000000
	O	1.121223	1.655486	0.000000	1.121989	-2.316180	0.000000
	C	-0.346463	0.235668	1.256401	-0.276615	-0.847802	-1.266320
	C	-0.346463	0.235668	-1.256401	-0.276615	-0.847802	1.266320
	H	-0.308293	-0.863229	-1.129100	-0.168572	0.242011	1.220332
	H	0.188322	0.603971	-2.127543	0.223376	-1.277205	2.129239
	H	-1.402663	0.502707	-1.326362	-1.348396	-1.043761	1.318508
	H	0.188322	0.603971	2.127543	0.223376	-1.277205	-2.129239
	H	-1.402663	0.502707	1.326362	-0.168572	0.242011	-1.220332
	H	-0.308293	-0.863229	1.129100	-1.348396	-1.043761	-1.318508
	X	-0.346463	-2.384391	0.000000	-0.276615	2.439205	0.000000
		$F\cdots CH_3COCH_3$			$Cl\cdots CH_3COCH_3$		
C_1 Neutral	C	0.000000	0.000000	0.000000	-1.047901	-0.066772	-0.009704
	O	0.000000	0.000000	1.218360	-0.115516	-0.855880	-0.025581
	C	1.285316	0.000000	-0.783839	-0.851794	1.421213	-0.010007
	C	-1.274141	-0.000570	-0.800298	-2.467003	-0.561940	0.019214
	H	-1.300052	0.874338	-1.448509	-3.023193	-0.061489	0.809927
	H	-2.133333	0.000309	-0.140045	-2.487872	-1.636376	0.161184
	H	-1.300363	-0.877073	-1.446355	-2.948609	-0.306181	-0.924156
	H	2.133712	-0.001165	-0.108855	0.175123	1.672241	-0.247818
	H	1.323432	0.876740	-1.428880	-1.094248	1.798781	0.983696
	H	1.322458	-0.875303	-1.430869	-1.538718	1.892819	-0.709701
	X	-2.030321	-0.000908	2.409032	2.237755	-0.074574	0.007912

Table S11: Cartesian coordinates of the geometries of bromide and iodide-acetone complexes optimised at MP2/AVQZ, in Å.

		$\mathrm{Br^{-}\cdots CH_3COCH_3}$			$\mathrm{I^{-}\cdots CH_3COCH_3}$		
		x	y	z	x	y	z
C_s Anion	C	1.212073	-1.819105	0.000000	1.496803	-2.295964	0.000000
	O	1.195279	-3.043359	0.000000	1.484088	-3.519657	0.000000
	C	1.212073	-1.016555	1.266933	1.496803	-1.495167	1.268534
	C	1.212073	-1.016555	-1.266933	1.496803	-1.495167	-1.268534
	H	0.386579	-0.297198	-1.226292	0.665043	-0.784381	-1.242101
	H	1.142990	-1.672187	-2.129542	1.439242	-2.153074	-2.130059
	H	2.126163	-0.423759	-1.318269	2.404023	-0.892017	-1.316041
	H	1.142990	-1.672187	2.129542	1.439242	-2.153074	2.130059
	H	0.386579	-0.297198	1.226292	0.665043	-0.784381	1.242101
	H	2.126163	-0.423759	1.318269	2.404023	-0.892017	1.316041
	X	-1.105457	1.492756	0.000000	-0.902486	1.274226	0.000000
		$\mathrm{Br\cdots CH_3COCH_3}$			$\mathrm{I\cdots CH_3COCH_3}$		
C_1 Neutral	C	-1.706026	-0.066764	-0.019257	-2.197741	-0.068471	-0.009041
	O	-0.766297	-0.846557	-0.058511	-1.247068	-0.835827	-0.026016
	C	-1.519233	1.422467	-0.017936	-2.026545	1.422874	-0.009261
	C	-3.119157	-0.573761	0.040964	-3.606267	-0.590310	0.019882
	H	-3.663756	-0.074136	0.840274	-4.170200	-0.106958	0.815777
	H	-3.127522	-1.647705	0.187981	-3.605277	-1.665965	0.154425
	H	-3.621926	-0.326633	-0.893686	-4.096560	-0.337776	-0.919933
	H	-0.509675	1.680443	-0.316944	-0.996367	1.687635	-0.220874
	H	-1.694842	1.786898	0.994756	-2.301732	1.803456	0.974684
	H	-2.251425	1.900130	-0.665281	-2.698769	1.881871	-0.731552
	X	1.687600	-0.035377	0.008525	1.411864	-0.021891	0.002380